

## Identification and Reduction of Retracker-Related Noise in Altimeter-Derived Sea Surface Height Measurements

EDWARD D. ZARON

*Department of Civil and Environmental Engineering, Portland State University, Portland, Oregon*

ROBERT DECARVALHO\*

*NASA Jet Propulsion Laboratory, Pasadena, California*

(Manuscript received 11 August 2015, in final form 12 October 2015)

### ABSTRACT


Data from the *Jason-2* calibration/validation mission phase have been analyzed to identify the correlation between sea surface height (SSH) and significant wave height (SWH) errors. A cross-spectral analysis indicates that the SSH and SWH errors are nearly white and significantly correlated at scales from 12 to 100 km, consistent with the hypothesized error source, the waveform retracker. Because of the scale separation between the SWH signal and noise, it is possible to correct the SSH data by removing the SSH noise correlated with the SWH noise. Such a correction has been implemented using the empirical correlation found during the *Jason-2* calibration orbit phase and applied to independent data from other phases of the *Jason-1* mission. The efficacy of the correction varies geographically, but variance reductions between 1.6 and 2.2 cm<sup>2</sup> have been obtained, corresponding to reductions of 20%–27% in the noise floor of along-track spectra. The corrections are obtained from and applied to conventional, 1 Hz, altimetry data and lead to improvements in the signal-to-noise ratio for identification of high-frequency narrowband processes—for example, internal tides—from these data.

### 1. Introduction

The measurement principle of conventional nadir-looking pulse-compression satellite altimetry involves fitting a parametric model to averaged returned waveforms to obtain parameters that yield the best-fitting model (Chelton et al. 2001). The waveforms are equivalent to the record of electromagnetic energy returned as a function of time during the epoch of the transmitted pulse, as in pulse-limited radar altimetry (Chelton et al. 1989), and they may be represented as the convolution of separate models for the antenna gain function, the sea surface radar scattering cross section, and the sea

surface roughness (Brown 1977). Once found, the waveform parameters—for example, the central time of the rising edge of the waveform, the slope of the leading edge, the total power received, and the slope of the trailing edge—are converted to measurements of geophysical interest, the most common being the satellite range, significant wave height, and near-surface wind speed. The identification of parameters from recorded waveforms is referred to as retracking (Rodríguez and Martin 1994), and it is the method used to obtain geophysical measurements from modern altimeter systems. Waveforms are recorded and may be retracked at different rates, depending on the design of the satellite system, but for the Jason missions the standard Geophysical Data Records (GDR) are computed by retracking waveforms stored at 20 Hz, with geophysical values reported as 1-s averages (Picot et al. 2008). A variety of waveform models and parameter estimation algorithms have been employed for retracking that account for characteristics of the antenna, the scene illuminated by the radar pulse, and approximations to the physics of the ocean surface and its electromagnetic properties (Rodríguez 1988; Zanifé et al. 2003; Thibaut et al. 2010). For the *Jason-1* (J1) and

---

 Denotes Open Access content.

---

\* Current affiliation: Ambition Inc., Chattanooga, Tennessee.

---

*Corresponding author address:* E. D. Zaron, Department of Civil and Environmental Engineering, Portland State University, P.O. Box 751, Portland, OR 97207-0751.  
E-mail: ezaron@pdx.edu

DOI: 10.1175/JTECH-D-15-0164.1

*Jason-2* (*J2*) missions, the GDR data values are obtained with a four-parameter maximum likelihood estimator retracker (MLE4) based on the Brown waveform model (Amarouche et al. 2004).

The measurements of the satellite range obtained by waveform retracking are converted to measurements of sea surface height (SSH) relative to some reference surface using the satellite position (precise orbit determination), properties of the atmosphere (path delay effects), and information about ocean surface wave dynamics and electromagnetic properties (sea state bias). Additional corrections to the retrieved SSH generally involve removal or transformation of other, possibly time variable, reference surfaces, such as the tide (Chelton et al. 2001; Picot et al. 2008).

One consequence of the waveform retracking algorithm is that random errors in waveform data, and systematic errors in the waveform model, can lead to correlated errors in the derived geophysical measurements. For example, Sandwell and Smith (2005) hypothesized that conventional three-parameter waveform retracking leads to correlated errors in SSH and significant wave height (SWH), and that by spatially smoothing the SWH along the track, one could use a second pass of two-parameter retracking, where the SWH is treated as a known, to improve the precision of the two estimated parameters, range and returned power. Garcia et al. (2014) implemented this approach and found that the noise floor can be reduced by approximately 30%, which significantly improves the effective spatial resolution of the SSH. For their application, which involved estimating the slope of the mean sea surface to estimate the near-Earth gravity field, the lower-noise SSH estimates led to more precise gravity field estimates down to 40-km wavelength.

The approach taken in this paper is similar to that taken in Garcia et al. (2014), except that the error correlation between SSH and SWH is diagnosed empirically, rather than being inferred from the properties of the waveform model and parameter estimation algorithm, and a correction is developed for and applied to a standard 1-Hz data product. The correlated errors are diagnosed from the *J1* and *J2* altimeters during the *J2* calibration/validation phase, when *J1* observed the sea surface from the same orbit as *J2*, delayed by 55 s. The two independent measurements of essentially the same sea surface are then differenced to yield time series of measurement errors. It is assumed that retracker noise is the dominant error in this series, and the empirical correlation is used to develop a correction that decorrelates the SSH and SWH errors. Variance reductions of 20%–27% of the SSH noise level are obtained when the correction is applied to independent data from other orbit phases.

TABLE 1. Orbits, path delay corrections, and geophysical corrections. Identical sources for corrections are used for both *J1* and *J2* missions. Source names follow the usage in RADS. MOG2D stands for the Modèle d'Onde de Gravité à 2 Dimensions. GOT stands for the Goddard/Grenoble Ocean Tide. DTU10 stands for the Technical University of Denmark 10-MW reference wind turbine.

Parameter	Source
Orbit altitude	GDR-D
Dry troposphere	ECMWF
Wet troposphere	Radiometer
Ionosphere	Smoothed dual frequency
Inverse barometer	MOG2D dynamic atmosphere
Solid Earth tide	Cartwright, Taylor, Edden
Ocean tide	GOT4.8
Load tide	GOT4.8
Pole tide	Wahr
Sea-state bias	CLS nonparametric
Mean sea surface	DTU10

This paper is organized as follows. First, the data utilized are discussed in more detail, including the suite of routine corrections applied prior to determination of the SSH and SWH correlation. Then, the correlation between the SSH and SWH errors is exhibited using dual-satellite differences from the calibration/validation orbit phase, and the correlation is shown to be similar to that which could be diagnosed from single-satellite collinear differences. It is then shown that the correlation varies as a function of SWH, and this fact is used to develop a single-parameter model for correcting the SSH assuming the high-frequency SWH data consists entirely of retracker error. Finally, the correction is validated using independent data from other locations and *J1* mission phases, and the implications of the study are discussed.

## 2. Data

The satellite altimeter data, orbits, and environmental corrections used in this study were extracted from the Radar Altimetry Database System (RADS; Naeije et al. 2002; Scharroo et al. 2013; <http://rads.tudelft.nl/rads/rads.shtml>). The suite of SSH corrections corresponding to the GDR, version D (GDR-D), standards have been applied (Picot et al. 2014), as listed in detail in Table 1. One potentially relevant point of note is that a multiparameter empirical sea state bias (SSB) correction is applied (Labroue et al. 2004). Because the development of the SSB correction involves, in part, removing the correlation between SSH and SWH, it will have some impact on the short-wavelength components of these fields, which are the focus of the present study. Thus, one expects the coefficients of the proposed retracker-related corrections to be

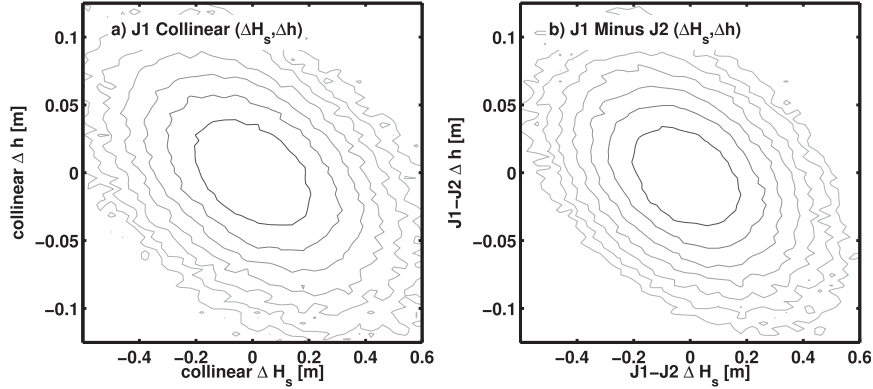


FIG. 1. SSH ( $h$ ) vs SWH ( $H_s$ ) histograms. (a) Along-track collinear differences of SSH and SWH from the *J1* mission illustrate the negative correlation between these quantities at short scales. (b) Differences between the *J1* and *J2* missions during the calibration/validation orbit phase are also correlated. Contours correspond to the integrated probability of the enclosed area in the following sequence: 0.50, 0.75, 0.875, . . . .

influenced by the details of the SSB correction. Presumably, at some point in the future, SSB and retracker-related corrections could be rederived independently.

Data from the *J2* calibration/validation orbit phase are utilized from 4 July 2008 to 26 January 2009. The retracker-related error correlation is diagnosed from data in the North Atlantic, within  $30^{\circ}$ – $55^{\circ}$ N,  $15^{\circ}$ – $45^{\circ}$ W, where the range of SWH variability is sufficient to estimate a SWH-dependent correlation between SWH and SSH. The proposed correction is tested within domains in the tropical and subtropical North Pacific, and it is validated against independent *J1* data collected prior to the calibration/validation period, from 15 February 2002 to 15 June 2008. The performance of the correction is measured by the reduction of the high-wavenumber noise floor of along-track power spectra, as well as by variance reductions in single-satellite cross-over differences.

### 3. Results

One observation that prompted the present study is shown in Fig. 1a, which shows the two-dimensional histogram of collinear differences (i.e., first differences of quantities along the satellite ground track) of SSH, denoted  $\Delta h$ , and SWH, denoted  $\Delta H_s$ . The first differences filter out long-wavelength signals and emphasize small-scale noise, and it is apparent that the noise is anticorrelated; positive SWH increments are associated with negative SSH increments. Further evidence that the correlation is caused by noise is presented in Fig. 1b, where dual-satellite differences between the *J1* and *J2* missions during the calibration/validation orbit phase

are shown. The same environmental corrections are applied to *J1* and *J2* SSH, so the dual-satellite differences ought to be a good measure of measurement noise.

The correlation between small-scale SSH and SWH has been noted previously (DeCarvalho et al. 2011). It is hypothesized that the correlation is caused by the correlated estimation error in the retracker algorithm rather than, say, the sea state bias. Garcia et al. (2014) have analyzed the random errors in retrackerers based on least squares fitting to the Brown waveform model, and their Table 2 reports values for the covariance of travel time  $\tau$  and the surface roughness parameter  $\sigma$ . These parameters are linearly related to SSH and SWH, respectively, and the tabulated values correspond to an SWH-dependent correlation between SSH and SWH errors ranging from  $-0.23$  at  $H_s = 2$  m to  $-0.39$  at  $H_s = 6$  m. The correlation of the data in Fig. 1 is about  $-0.3$ , which is within the range reported in Garcia et al. (2014). Here and below, the symbols  $h$  and  $H_s$  represent SSH and SWH data values, respectively.

Assuming the quantities  $\Delta h$  and  $\Delta H_s$  formed by differencing *J1* and *J2* during the calibration orbit phase consist entirely of error permits one to develop a linear model,

$$\Delta h = \rho \Delta H_s, \quad (1)$$

where the coefficient  $\rho$  may be determined by total least squares regression (Van Huffel 1989), appropriate since both  $\Delta h$  and  $\Delta H_s$  contain error. Consistent with the hypothesized source of the error, the coefficient of proportionality displays dependence on SWH, and it is represented as

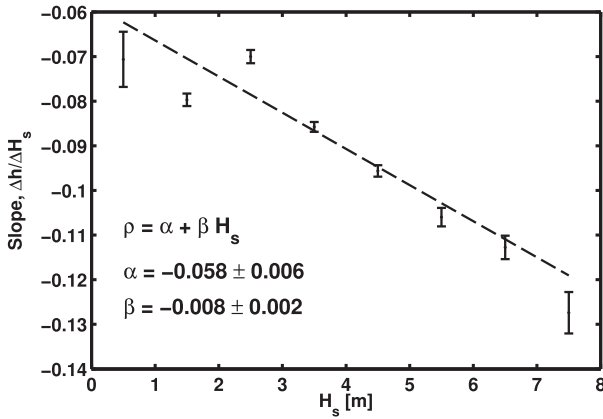


FIG. 2. Total least squares regression has been used to find a relation,  $\Delta h = \rho \Delta H_s$ , from the data shown in Fig. 1b, by binning the data within ranges of  $H_s$ . The coefficient  $\rho$  is expressed parametrically in terms of  $H_s$  as  $\rho = \alpha + \beta H_s$ , shown by the dashed line. Confidence intervals for the regression coefficients,  $\alpha$  and  $\beta$ , have been computed using the bootstrap (Efron 1987).

$$\rho = \alpha + \beta H_s, \quad (2)$$

graphed in Fig. 2. By binning  $\Delta h$  and  $\Delta H_s$  within ranges of SWH, values for the coefficients are found to be  $\alpha = -0.058$  and  $\beta = -0.008 \text{ m}^{-1}$ . We reiterate that specific values of the numeric constants obtained here depend in detail on the waveform retracker and SSB correction employed in GDR-D, and that the correction coefficients may need to be recomputed if either of these are changed in subsequent versions of the GDR.

With the above-mentioned relationship between errors in SSH and SWH, it is possible to develop a correction to reduce retracker-related noise in SSH. Let the corrected SSH  $h_c$  be defined as

$$h_c = h - \rho H'_s, \quad (3)$$

where  $H'_s$  is an estimate of the retracker-related SWH noise. The high coherence and stable phase lag between  $J1$  minus  $J2$  increments of SSH and SWH suggest that SWH is essentially all noise at wavelengths shorter than 100 km (Fig. 3). Thus, low-pass filtering SWH should lead to more accurate estimates of  $H_s$ , denoted  $\bar{H}_s$ , as well as an estimate of the SWH noise,  $H'_s = H_s - \bar{H}_s$ . To reduce the influence of SWH error on the correction coefficient  $\rho$  the low-passed SWH,  $\bar{H}_s$  is used in place of  $H_s$  in Eq. (2).

Note that the analysis of coherence for the calibration/validation mission phase requires some care in handling missing data. It was found that the coherence estimates are sensitive to interpolation across data gaps and, consequently, only gap-free segments are used in the coherence calculations. Spectral analysis is performed

using Welch's method on records of length 780 km using one-half overlap using the Hann window.

The proposed SSH correction requires a distinction between SWH signal and SWH noise, which is here implemented with a simple high-pass filter. Previous studies of SWH from the *J1* calibration/validation mission phase, when *J1* and TOPEX/Poseidon flew in the same orbit separated by 70 s, found that altimeter-derived SWH estimates were dominated by noise at scales smaller than 100 km (Ray and Beckley 2003); although, this is somewhat more pessimistic than the 60-km scale inferred from a nonlinear filter applied to *Geosat* SWH observations (Tournadre 1993). The two-pass retracker employed by Garcia et al. (2014) uses a 90-km filter cutoff. Fortunately, the performance of the proposed correction depends weakly on the assumed cutoff wavelength for scales from 50 to 150 km, resulting in changes of only a few tenths of squared centimeters in variance reduction. For the examples below, a filter with a half-power wavelength of 100 km and a  $k^{-2}$  roll-off rate is used.

The results of applying the above-described correction to SSH are shown in Fig. 3. The notation  $\Delta h$  refers to SSH differences,  $J1$  minus  $J2$ , measured by the missions during the calibration/validation phase. The coherence between SSH and SWH differences drops from 0.4 without the correction to less than 0.1 with the correction (Fig. 3a). The reduction of coherence does not just occur with the errors. Figure 3b shows that the coherence of  $J1$  SSH and SWH data also drops with the correction. To emphasize the robustness of the correlation between SSH and SWH, Fig. 3c shows the phase lag of the cross spectrum. It illustrates the  $180^\circ$  phase lag—that is, change of sign—between the correlated components, as was apparent in Fig. 1. The corrected SSH displays no stable phase relationship with SWH, as expected (not shown).

Figure 4 illustrates the wavenumber spectra of SSH and SWH prior to making the correction. The spectrum of  $\Delta h$ ,  $S(\Delta h)$ , contains noise from both altimeters, so one-half its value is plotted as an empirical estimate of the noise spectrum (Fig. 4a). Note that  $S(\Delta h)$  is dominated by retracker noise since errors in the environmental and mean sea surface corrections cancel in  $\Delta h$ . The spectrum of  $J1$  SSH  $S(h)$  drops to about twice the  $S(\Delta h)/2$  at a wavelength of 80 km. The spectrum of SWH and its noise indicates that  $S(H_s)$  is equal to twice the noise spectrum  $S(\Delta H_s)$  at about 100-km wavelength. The smooth dashed and dashed-dotted curves below  $S(H_s)$  illustrate the spectra of  $H'_s$  and  $\bar{H}_s$ , respectively, which are used to define  $\rho$  and  $h_c$  in Eq. (3), respectively.

The spectra of the original and corrected SSH for *J1* in the North Atlantic region are compared in Fig. 5a. One

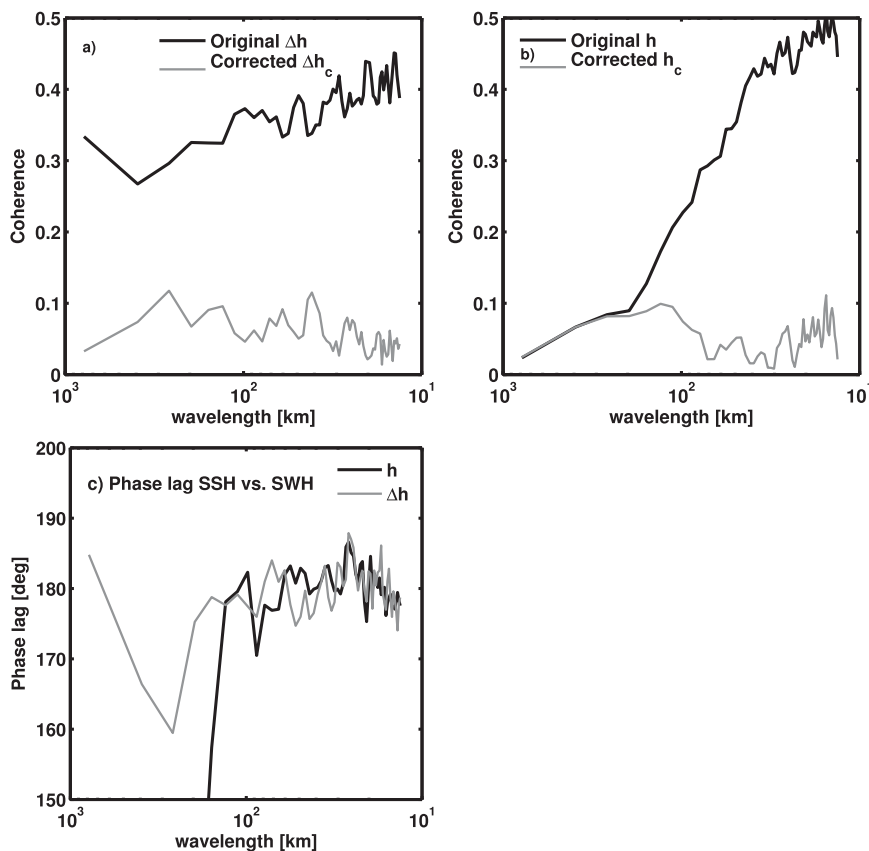


FIG. 3. Cross-spectral statistics. (a) The coherence spectrum of SSH and SWH is shown for the  $J1 - J2$  differences from the calibration/validation orbit phase for both the original SSH  $\Delta h$  and the corrected SSH  $\Delta h_c$ . (b) The coherence spectrum of SSH and SWH data shows the correlation of  $h$  and  $H_s$  for scales shorter than 100 km; the  $h_c$  is not significantly correlated with SWH. (c) The phase lag computed from the cross spectrum indicates the unambiguous sign reversal (anticorrelation) between the correlated components of SSH and SWH.

can see that  $S(h)$  and  $S(h_c)$  are nearly identical at wavelengths longer than about 80 km, but at smaller scales the noise floor of  $S(h)$  is reduced. The high-frequency noise floor has been lowered by 27% in this case, which is also reflected in the reduced empirical noise spectrum,  $S(\Delta h_c)/2$ . The reduction of  $S(\Delta h_c)$  is noteworthy since the corrections to the  $J1$  and  $J2$  data are computed independently. Figure 5b illustrates the same spectra for data from a test region in the North Pacific ( $20^\circ$ – $45^\circ$ N,  $205^\circ$ – $235^\circ$ E). In this case the noise floor is reduced by about 20%.

The above-described tests have applied the proposed correction to data from the calibration/validation orbit phase when an independent estimate of the SSH and SWH errors is available, namely, the dual-satellite differences. Further validation of the correction is provided by applying it to independent  $J1$  data coming from orbit cycles 5–255, before the  $J2$  calibration/validation phase. The first example illustrates  $J1$  data from within the original test region in the North Atlantic, now using

far more data (Fig. 6a). The results are very similar to those obtained during the calibration/validation phase. The correction results in a  $2.2 \text{ cm}^2$  reduction in SSH variance, corresponding to a 24% reduction in the noise level. A more stringent, and independent, test involves the reduction in variance of crossover differences. In this case the variance reduction is identical,  $2.2 \text{ cm}^2$ .

Figure 6b illustrates the impact of the correction at a region centered on the Hawaiian Ridge ( $16^\circ$ – $28^\circ$ N,  $190^\circ$ – $198^\circ$ E). This region was chosen because the SSH spectrum is relatively shallow and contains short-wavelength features attributed to the internal tide (Ray and Mitchum 1996). In this case the variance reduction is  $1.6 \text{ cm}^2$ , corresponding to a reduction in the noise floor of 23%. The crossover variance reduction is similar,  $1.7 \text{ cm}^2$ . The final example shown in Fig. 6c is the along-track spectrum for pass number 249, which passes through French Frigate Shoals, an internal tide-generation site. The quantitative variance reduction statistics are the same as those of the larger Hawaiian Ridge region, and the example serves to

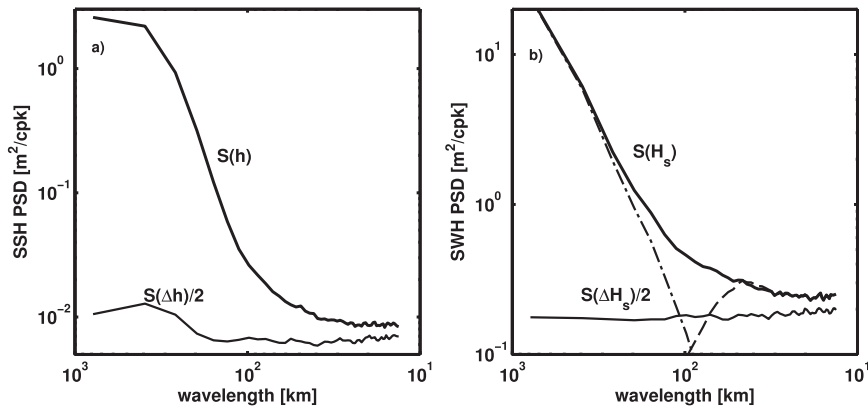


FIG. 4. SSH and SWH spectra from the North Atlantic. (a) Spectra of  $J1$  SSH  $S(h)$  (heavy line) and  $J1 - J2$  SSH difference during the calibration/validation phase  $S(\Delta h)$  (scaled by one-half to estimate the noise level). (b) Spectra of  $J1$  SWH  $S(H_s)$  (heavy line) and  $J1 - J2$  SWH difference  $S(\Delta H_s)$  (scaled by one-half). The spectra of the low-pass  $\bar{H}_s$  (dashed-dotted) and high-pass  $H'_s$  (dashed) SWH intersect at approximately 100 km.

illustrate how the reduced noise floor increases the signal-to-noise ratio of the spectral peak associated with the internal tide near 75-km wavelength.

#### 4. Discussion

The empirical correlation between SSH and SWH errors found here, as inferred from dual-satellite differences, is in agreement with the correlation previously predicted by analysis of retracker algorithms (Sandwell and Smith 2005), and inferred from variance reduction statistics with single-satellite data (Garcia et al. 2014). Based on the assumption that retracker-derived SWH values are dominated by noise at small scales, the noise floor of SSH has been reduced by removing the SSH component that is correlated with the SWH noise.

Separation of SWH signal and noise is accomplished with a simple along-track low-pass filter and its complement, making the noise correction feasible to apply to conventional 1-Hz altimetry data. Because Garcia et al. (2014) assess SSH variance reductions using 20-Hz retracked data, it is not possible to make an unambiguous comparison with the present approach; although, variance reductions found here appear to be consistent with their results.

The results obtained here replicate earlier findings obtained by analysis of single-satellite residuals (DeCarvalho et al. 2011), where a figure nearly identical to Fig. 1a is presented in the context of developing a family of sea state bias models. The hypothesis that “variance reductions are likely the result of removing correlation between range measurement noise and SWH

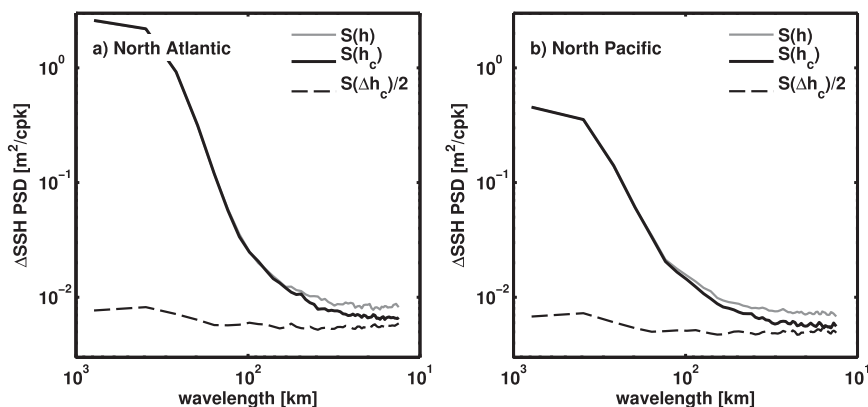


FIG. 5. SSH summary spectra. Panels compare the spectrum of original data  $S(h)$  (solid gray line) the corrected data  $S(h_c)$  (black line), and error spectrum  $J1 - J2$   $S(\Delta h_c)/2$  (dashed gray line). (a) North Atlantic: 27% reduction in noise level. (b) North Pacific: 20% reduction in noise level.



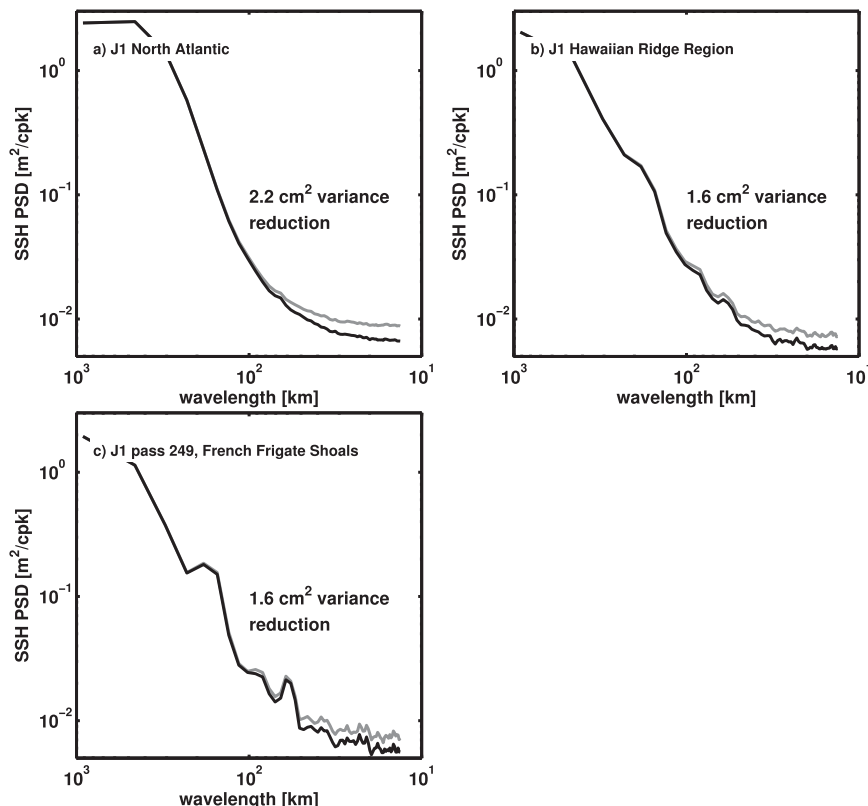


FIG. 6. Verification of the correction. Results of using the proposed retracker error correction are shown for independent data not used to develop the correction. (a) SSH spectra in the North Atlantic region using *J1* data from orbit cycles 5–255, prior to the *J2* calibration/validation phase. (b) Spectra of *J1* SSH from a region around the Hawaiian Ridge. (c) Spectra of *J1* SSH from pass number 249, which passes over French Frigate Shoals, a generation site of large-amplitude internal tide. The light line shows uncorrected spectrum  $S(h)$ ; the heavy line shows corrected spectrum  $S(h_c)$ .

measurement noise” (DeCarvalho et al. 2011) is supported by the present methodology, which employed dual-satellite differences, an unambiguous measure of noise. The variance explained by the two approaches is virtually identical and suggests the proposed approach could be applied to other missions with regression coefficients determined from single-satellite data.

The quantitative significance of the proposed correction is to reduce the noise floor of along-track SSH by 20%–27%, which reduces the smallest wavelength resolvable by 1-Hz altimetry, depending on the slope of the spectrum. The practical utility of the noise reduction depends on the intended application of SSH data, but it is expected that it will significantly improve the signal-to-noise ratio for identification of higher-than-mode-1 internal tides from altimetry (Ray and Zaron 2015).

More broadly, the present work contributes to understanding the causes and magnitudes of different noise sources in altimetry. Inferences about ocean

dynamics based on the SSH wavenumber spectrum are sensitive to assumptions regarding the spectrum of noise at high wavenumbers (Stammer 1997; Xu and Fu 2011). The high wavenumber noise floor of conventional 1-Hz pulse-width-limited altimetry is caused by spatial inhomogeneity in the radar footprint, which causes systematic deviations between the measured and theoretical Brown waveform (Dibarboure et al. 2014). The noise caused by the spatial inhomogeneity is correlated between consecutive 20-Hz waveforms, leading to a noise floor that is higher than would be obtained from uncorrelated noise. Because the spatial inhomogeneity causes waveforms to deviate from the Brown model when there are small-scale “sigma blooms” within the radar footprint (Mitchum et al. 2004), it may be that these regions contribute disproportionately to the SSH and SWH error correlation. In any event, the present work indicates the magnitude of one component of SSH error and a straightforward procedure to reduce or eliminate it.

The proposed correction relies on knowledge of SWH noise to remove correlated noise in SSH. What if the SWH noise is not estimated correctly, and the proposed correction is contaminating the SSH with SWH signal? For example, simultaneous jumps in SSH and SWH have been observed across narrow, 50 km, ocean fronts (McClain et al. 1982). There are two considerations that suggest this is not a problem. First, the phase cross spectrum shown in Fig. 3c is fully consistent with the assumption that  $H_s$  is dominated by noise for wavelengths smaller than 100 km. It is difficult to imagine a physical process that would lead to high coherence and stable phase over the high wavenumbers but not the lower wavenumbers. Second, the reduction in crossover variance suggests that the SSH correction is valid, as the separation into low- and high-pass SWH  $\bar{H}_s$  and  $H'_s$  is performed independently along each ascending and descending track. Ideally, it would be best to locally modify the filter scale to optimally estimate the SWH noise, but at present it is unclear how to account for temporal or geographic variability in this quantity.

The SSB correction is another SSH correction that, by design, decorrelates  $\Delta h$  and  $\Delta H_s$ , where the increments are typically evaluated between orbit cycles (Gaspar et al. 2002; Labroue et al. 2004; Tran et al. 2006). To assess the impact of the along-track correction on the intercycle increments, Fig. 7 illustrates the two-dimensional probability density function (pdf) of  $(\Delta h_c, \Delta H_s)$  for cycles 1–254 of the *J2* mission, taking the differences between consecutive cycles. The primary influence of the proposed correction is to reduce the spread of the pdf in the second and fourth quadrants, where  $\Delta H_s$  and  $\Delta h$  are anticorrelated,  $\Delta H_s \propto -\Delta h$ , and to make the pdf more symmetrical for positive and negative increments. In other words, letting  $P$  denote probability density, the change results in the condition  $|P(\Delta H_s, \Delta h) - P(\Delta H_s, -\Delta h)| > |P(\Delta H_s, \Delta h_c) - P(\Delta H_s, -\Delta h_c)|$ , with a similar result for reflections in  $\Delta H_s$ . Note that the magnitude of the variance reduction of the proposed correction is comparable to the variance reductions of multidimensional sea state bias models as compared with the unidimensional correction,  $-3.8\%$  of  $H_s$  (Tran et al. 2010). At some point it may be possible to decompose the joint pdf of  $(\Delta h, \Delta H_s)$  into correlated, uncorrelated, and independent components according to the physics of the sea surface and the retracker estimation algorithms, thus forming a logical basis for devising better SSH correction algorithms. But, until that can be done, it may be advisable to separately quantify retracker-related and physical (electromagnetic bias, skewness bias, etc.) causes of SWH and SSH correlation when designing new SSB corrections.

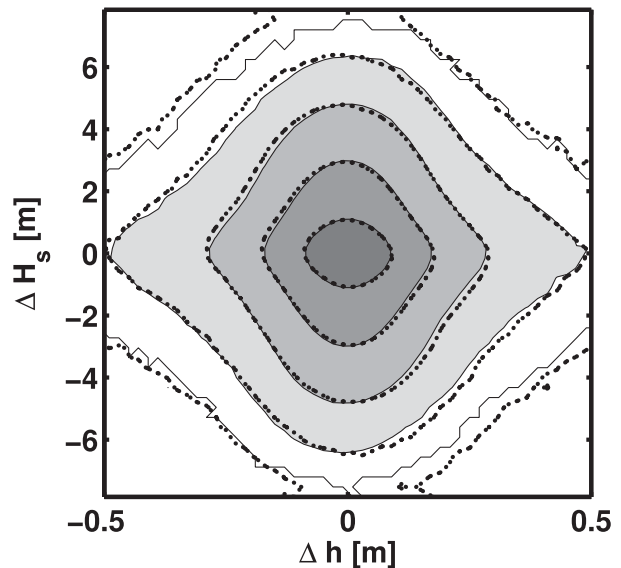


FIG. 7. The joint pdf of 10-day SSH and SWH increments for the *J2* mission. The solid contours and grayscale show the  $(10^{-4}, 10^{-3}, \dots, 1)$  pdf isolines for the corrected data,  $(\Delta h_c, \Delta H_s)$ , where the increments are evaluated between consecutive orbit cycles. The dashed line shows the same isolines for the uncorrected data  $(\Delta h, \Delta H_s)$ . The main effect of the correction is to reduce the spread within the anticorrelated quadrants  $\Delta H_s \propto -\Delta h$ .

## 5. Summary

Observation of a correlation between small-scale noise in SSH and SWH motivated the development of a correction for SSH that seeks to decorrelate the small-scale signals in SSH and SWH. The proposed correction is developed by hypothesizing that the correlated noise results from the algorithm that estimates geophysical parameters from the radar waveforms, the retracker, the correlation deriving from the non-orthogonal sensitivities of the waveform model to physical parameters (Brown 1977; Sandwell and Smith 2005). Based on the assumption that noise dominates the SWH signal at wavelengths shorter than 100 km, a correction to SSH was derived with a SWH-dependent model of the error correlation.

The error correlation model and the correction were initially developed using collinear dual-satellite SSH and SWH differences from the North Atlantic during the calibration/validation phase of the *J2* altimeter mission, when *J2* followed *J1* on the same ground track. The correction was validated in the tropical and subtropical North Pacific using data from the calibration/validation phase as well as earlier, independent, *J1* data. Analysis of along-track spectra found that the empirical correction reduced the SSH noise level by 20%–27%, equivalent to a variance reduction of  $1.6$ – $2.2 \text{ cm}^2$ . Similar variance reduction statistics were obtained from an analysis of crossover differences.



The correlation between SSH and SWH caused by waveform retracking is not orthogonal to the physical correlation of these quantities resulting from the SSB. It would be valuable to investigate how the proposed empirical correction for retracker-related SSH error depends on the underlying SSB corrections; however, this is a complex task given the diversity of approaches to SSB modeling and their development. The proposed correction contributes to a better understanding of short-wavelength altimetry errors and ought to contribute to improved identification of sub-100-km-scale features in conventional altimetry.

**Acknowledgments.** This project was supported by the National Geospatial-Intelligence Agency Academic Research Program (NARP) project “Improving Coastal Marine Gravity.” The authors would like to acknowledge the important contribution of Dr. Douglas Vandemark, who suggested the cross-spectral analysis of SSH and SWH after reviewing an early version of this manuscript.

## REFERENCES

- Amarouche, L., P. Thibaut, O. Z. Zanifé, J.-P. Dumont, P. Vincent, and N. Steunou, 2004: Improving the Jason-1 ground retracking to better account for attitude effects. *Mar. Geod.*, **27**, 171–197, doi:[10.1080/01490410490465210](https://doi.org/10.1080/01490410490465210).
- Brown, G., 1977: The average impulse response of a rough surface and its applications. *IEEE Trans. Antennas Propag.*, **25**, 67–74, doi:[10.1109/TAP.1977.1141536](https://doi.org/10.1109/TAP.1977.1141536).
- Chelton, D. B., E. J. Walsh, and J. L. MacArthur, 1989: Pulse compression and sea level tracking in satellite altimetry. *J. Atmos. Oceanic Technol.*, **6**, 407–438, doi:[10.1175/1520-0426\(1989\)006<0407:PCASLT>2.0.CO;2](https://doi.org/10.1175/1520-0426(1989)006<0407:PCASLT>2.0.CO;2).
- , J. C. Ries, B. J. Haines, L.-L. Fu, and P. S. Callahan, 2001: Satellite altimetry. *Satellite Altimetry and Earth Sciences: A Handbook of Techniques and Applications*, L.-L. Fu and A. Cazenave, Eds., International Geophysics Series, Vol. 69, Academic Press, 1–131.
- DeCarvalho, R., S. D. Desai, and B. J. Haines, 2011: A nonparametric sea state bias model based on SWH and Sigma0: Extending to three dimensions. *Ocean Surface Topography Science Team Meeting*, San Diego, CA, NASA. [Available online at <http://www.aviso.altimetry.fr/fileadmin/documents/OSTST/2011/poster/Cavalho.pdf>.]
- Dibarboure, G., F. Boy, J. D. Desjonqueres, S. Labroue, Y. Lasne, N. Picot, J. C. Poisson, and P. Thibaut, 2014: Investigating short-wavelength correlated errors on low-resolution mode altimetry. *J. Atmos. Oceanic Technol.*, **31**, 1337–1362, doi:[10.1175/JTECH-D-13-00081.1](https://doi.org/10.1175/JTECH-D-13-00081.1).
- Efron, B., 1987: Better bootstrap confidence intervals. *J. Amer. Stat. Assoc.*, **82**, 171–185, doi:[10.1080/01621459.1987.10478410](https://doi.org/10.1080/01621459.1987.10478410).
- Garcia, E. S., D. T. Sandwell, and W. H. F. Smith, 2014: Retracking CryoSat-2, Envisat and Jason-1 radar altimetry waveforms for improved gravity field recovery. *Geophys. J. Int.*, **196**, 1402–1422, doi:[10.1093/gji/ggt469](https://doi.org/10.1093/gji/ggt469).
- Gaspar, P., S. Labroue, F. Ogor, G. Lafitte, L. Marchal, and M. Rafanel, 2002: Improving nonparametric estimates of the sea state bias in radar altimetry measurements of sea level. *J. Atmos. Oceanic Technol.*, **19**, 1690–1707, doi:[10.1175/1520-0426\(2002\)019<1690:INEOTS>2.0.CO;2](https://doi.org/10.1175/1520-0426(2002)019<1690:INEOTS>2.0.CO;2).
- Labroue, S., P. Gaspar, J. Dorandeu, O. Z. Zanifé, F. Mertz, P. Vincent, and D. Choquet, 2004: Nonparametric estimates of the sea state bias for the Jason-1 radar altimeter. *Mar. Geod.*, **27**, 453–481, doi:[10.1080/01490410490902089](https://doi.org/10.1080/01490410490902089).
- McClain, C. R., N. E. Huang, and P. E. LaViolette, 1982: Measurements of sea-state variations across oceanic fronts using laser profilometry. *J. Phys. Oceanogr.*, **12**, 1228–1244, doi:[10.1175/1520-0485\(1982\)012<1228:MOSSVA>2.0.CO;2](https://doi.org/10.1175/1520-0485(1982)012<1228:MOSSVA>2.0.CO;2).
- Mitchum, G. T., D. W. Hancock III, G. S. Hayne, and D. C. Vandemark, 2004: Blooms of  $\sigma^0$  in the TOPEX radar altimeter data. *J. Atmos. Oceanic Technol.*, **21**, 1232–1245, doi:[10.1175/1520-0426\(2004\)021<1232:BOITTR>2.0.CO;2](https://doi.org/10.1175/1520-0426(2004)021<1232:BOITTR>2.0.CO;2).
- Naeije, M., E. Doornbos, L. Mathers, R. Scharroo, E. Schrama, and P. Visser, 2002: Radar Altimeter Database System: Exploitation and extension (RADsxx). Tech. Rep. NUSP-2 Rep. 02-06, NUSP-2 Project 6.3/IS-66, Delft Institute for Earth-Oriented Space Research, 107 pp.
- Picot, N., K. Case, S. Desai, and P. Vincent, 2008: AVISO and PODAAC user handbook, IGDR and GDR Jason products, edition 4.1. AVISO Doc. SMM-MU-M5-OP-13184-CN, PODAAC Doc. JPL D-21352, 130 pp. [Available online at [http://podaac.jpl.nasa.gov/allData/jason1/L2/gdr\\_c/docs/Handbook\\_Jason\\_v4-1.pdf](http://podaac.jpl.nasa.gov/allData/jason1/L2/gdr_c/docs/Handbook_Jason_v4-1.pdf).]
- , S. Desai, J. Figa-Saldana, and R. Scharroo, 2014: Jason-2 version ‘D’ Geophysical Data Records: Public release. Aviso, 12 pp. [Available online at [http://www.aviso.oceanobs.com/fileadmin/documents/data/tools/JA2\\_GDR\\_D\\_release\\_note.pdf](http://www.aviso.oceanobs.com/fileadmin/documents/data/tools/JA2_GDR_D_release_note.pdf).]
- Ray, R. D., and G. T. Mitchum, 1996: Surface manifestation of internal tides generated near Hawaii. *Geophys. Res. Lett.*, **23**, 2101–2104, doi:[10.1029/96GL02050](https://doi.org/10.1029/96GL02050).
- , and B. D. Beckley, 2003: Simultaneous ocean wave measurements by the Jason and Topex satellites, with buoy and model comparisons. *Mar. Geod.*, **26**, 367–382, doi:[10.1080/714044527](https://doi.org/10.1080/714044527).
- , and E. D. Zaron, 2015:  $M_2$  internal tides and their observed wavenumber spectra from satellite altimetry. *J. Phys. Oceanogr.*, doi:[10.1175/JPO-D-15-0065.1](https://doi.org/10.1175/JPO-D-15-0065.1), in press.
- Rodriguez, E., 1988: Altimetry for non-Gaussian oceans: Height biases and estimation of parameters. *J. Geophys. Res.*, **93**, 14 107–14 120, doi:[10.1029/JC093iC11p14107](https://doi.org/10.1029/JC093iC11p14107).
- , and J. M. Martin, 1994: Assessment of the TOPEX altimeter performance using waveform retracking. *J. Geophys. Res.*, **99**, 24 957–24 969, doi:[10.1029/94JC02030](https://doi.org/10.1029/94JC02030).
- Sandwell, D. T., and W. H. Smith, 2005: Retracking ERS-1 altimeter waveforms for optimal gravity field recovery. *Geophys. J. Int.*, **163**, 79–89, doi:[10.1111/j.1365-246X.2005.02724.x](https://doi.org/10.1111/j.1365-246X.2005.02724.x).
- Scharroo, R., E. W. Leuliette, J. L. Lillibridge, D. Byrne, M. C. Naeije, and G. T. Mitchum, 2013: RADs: Consistent multi-mission products. *Proceedings of 20 Years of Progress in Radar Altimetry*, L. Ouwehand, Ed., ESA SP-710, CD-ROM.
- Stammer, D., 1997: Global characteristics of ocean variability estimated from regional TOPEX/POSEIDON altimeter measurements. *J. Phys. Oceanogr.*, **27**, 1743–1769, doi:[10.1175/1520-0485\(1997\)027<1743:GCOOVE>2.0.CO;2](https://doi.org/10.1175/1520-0485(1997)027<1743:GCOOVE>2.0.CO;2).
- Thibaut, P., J. C. Poisson, E. Bronner, and N. Picot, 2010: Relative performance of the MLE3 and MLE4 retracking algorithms on Jason-2 altimeter waveforms. *Mar. Geod.*, **33** (Suppl.), 317–335, doi:[10.1080/01490419.2010.491033](https://doi.org/10.1080/01490419.2010.491033).
- Tournadre, J., 1993: Time and space scales of significant wave heights. *J. Geophys. Res.*, **98**, 4727–4738, doi:[10.1029/92JC02625](https://doi.org/10.1029/92JC02625).
- Tran, N., D. Vandemark, B. Chapron, S. Labroue, H. Feng, B. Beckley, and P. Vincent, 2006: New models for satellite altimeter sea state bias correction developed using global wave model data. *J. Geophys. Res.*, **111**, C09009, doi:[10.1029/2005JC003406](https://doi.org/10.1029/2005JC003406).

- , —, S. Labroue, H. Feng, B. Chapron, H. L. Tolman, J. Lambin, and N. Picot, 2010: Sea state bias in altimeter sea level estimates determined by combining wave model and satellite data. *J. Geophys. Res.*, **115**, C03020, doi:[10.1029/2009JC005534](https://doi.org/10.1029/2009JC005534).
- Van Huffel, S., 1989: The extended classical total least squares algorithm. *J. Comput. Appl. Math.*, **25**, 111–119, doi:[10.1016/0377-0427\(89\)90080-0](https://doi.org/10.1016/0377-0427(89)90080-0).
- Xu, Y., and L. Fu, 2011: Global variability of the wavenumber spectrum of oceanic mesoscale turbulence. *J. Phys. Oceanogr.*, **41**, 802–809, doi:[10.1175/2010JPO4558.1](https://doi.org/10.1175/2010JPO4558.1).
- Zanifé, O. Z., P. Vincent, L. Amarouche, J. P. Dumont, and P. T. S. Labroue, 2003: Comparison of the Ku-band range noise level and the relative sea-state bias of the Jason-1, TOPEX, and Poseidon-1 radar altimeters. *Mar. Geod.*, **26**, 201–238, doi:[10.1080/714044519](https://doi.org/10.1080/714044519).